Enhanced Neurite Outgrowth and Regeneration in ALS Resistant Motor Neurons from SOD1 Mutant Mouse Models

Zachary B Osking[1], Jacob I. Ayers[2], Ryan Hildebrandt[3], Kristen Skruber[1], Hilda Brown[2], Danny Ryu[2], Amanda R. Eukovich[1], Todd E. Golde[2], David R. Borchelt[2], Tracy-Ann Read[1*] and Eric A. Vitriol[1*]

[1]Department of Anatomy and Cell Biology, [2]Department of Neuroscience, and [3]Department of Molecular Genetics and Microbiology, University of Florida, Gainesville, FL, USA, 32610

*To whom correspondence should be addressed: Tracy-Ann Read, taread@ufl.edu; Eric Vitriol, evitriol@ufl.edu

Abstract

Amyotrophic lateral sclerosis (ALS) is a progressive and fatal neurodegenerative disease characterized by motor neuron cell death and subsequent paralysis of voluntary muscles. Although ALS specifically affects motor neurons, some cells are resistant to disease progression. Most ALS studies have focused on the cellular mechanisms that cause loss of motor neuron viability. Less is known about the surviving neurons, and most of that information has come from gene expression profiling. In this study, we functionally characterize the surviving spinal motor neurons by culturing them from SOD1 ALS mouse models at various stages of disease progression. Surprisingly, we found that in comparison to non-transgenic controls, ALS resistant motor neurons from SOD1^{G93A} mice have enhanced axonal outgrowth and dendritic branching. They also display an increase in the number and size of actin-based structures such as growth cones and filopodia. The most substantial increase in outgrowth occurs in a low-copy SOD1^{G93A} model with delayed disease onset. This phenotype occurs independently of SOD1 enzymatic activity and is cell autonomous. Further, the enhanced outgrowth occurs before the mice become symptomatic, but increases with disease progression. These results indicate that ALS resistant motor neurons are primed for regeneration significantly before ALS symptoms are present. Understanding this mechanism of cellular resistance and increased axonal outgrowth could uncover new therapeutic targets for the treatment of ALS.

Keywords

Amyotrophic lateral sclerosis; SOD1, motor neuron, growth cone, actin, cytoskeleton

Abbreviations

ALS	Amyotrophic lateral sclerosis
MN	motor neuron
SOD1	superoxide dismutase 1
YFP	yellow fluorescent protein
NTg	non-transgenic
G93A	transgenic mouse line expressing SOD1 with a glycine-to-alanine mutation at position 93
G93A-DL	transgenic mouse line expressing SOD1 with a glycine-to-alanine mutation at position 93 with a lower copy number than the G93A mouse line
G85R	transgenic mouse line expressing SOD1 with a glycine-to-arginine mutation at position 85 fused to YFP

Introduction

Amyotrophic lateral sclerosis (ALS) is a fatal, adult-onset neurodegenerative disorder in which there is selective loss of motor neurons (MNs) in the cerebral cortex, brainstem and spinal cord [34]. Not all MNs are equally susceptible to cell death during ALS disease progression. ALS mostly targets MNs required for voluntary movement, whereas MNs of the autonomic system are less affected [54]. Certain groups of somatic motor neurons, including those in the oculomotor nucleus and Onuf's nucleus, are also generally spared [25,50,31,65]. Furthermore, there is a gradient of vulnerability among spinal MNs, where faster motor units become affected before slower muscle types [55]. MNs that are less ALS-susceptible can compensate for the cells that initially die by establishing new connections with the motor endplate, although many of these will eventually succumb to the disease [60].This selective neuronal vulnerability is present in both sporadic ALS and fALS and is also recapitulated in rodent models, such as the $SOD1^{G93A}$ mouse [50]. The mechanism that renders certain subgroups of MNs more susceptible to ALS is largely unknown, although studies have shown that ALS resistant MNs differentially express GABA and glutamate receptor subunits ([44], [43], [13]) show a higher expression of EGR1, IGF2 [3] and OPN [47]. On the other hand, ALS vulnerable motor neurons have high expression of matrix metalloproteinase-9 (MMP9) [11] which was identified as a modulator of ER stress [38,36], supporting previous studies showing that such ALS vulnerable MNs are selectively prone to ER stress [59].

Approximately 90% of ALS cases are sporadic with unknown etiology; the remaining 10% are inherited and known as familial ALS (fALS), of which over 20% have mutations in the gene encoding Cu/Zn superoxide dismutase 1 (SOD1) [14]. To date, over 155 different mutations have been identified in SOD1 either in isolated cases of ALS or more commonly in patients from families showing autosomal dominant patterns of inheritance [52,4]. ALS-linked SOD1 mutations are thought to induce a toxic gain-of-property of the protein, which becomes prone to misfolding and subsequent aggregation [37,57]. While the exact cause of SOD1-induced MN degeneration is unknown, a number of pathogenic processes, including excitotoxicity, oxidative stress, mitochondrial dysfunction, dysregulation of the cytoskeleton, axonal transport defects, and inflammation are considered to play important roles in eventually inducing cell death [22,33]. Some of the most significant advances in our understanding of how mutations in the SOD1 gene cause ALS have been achieved through rodent models. Since the generation of the first $SOD1^{G93A}$ transgenic mouse line [30], several other mutant SOD1 models now exist with slight variation in their pathologies, including time to onset of symptoms and death [15,35,49]. The $SOD1^{G93A}$ mouse (referred to here as G93A) carries 22 copies of a causative mutation (a glycine-to-alanine replacement at residue 93) in the human SOD1 gene, inserted randomly into chromosome 12 of the mouse genome [2]. This mouse model has an onset of paralysis at ~90 days, accompanied by degenerative motor neuron loss similar to that of human ALS pathology [62], and death by ~135 days depending on the genetic background and gender of the mice. The G93A mouse remains the most widely used model of human ALS [30] to date.

While most studies have focused on the cellular mechanisms and genes that induce MN death in ALS, less is known about the neurons that do survive, including their ability to resist stress-induced cell death and to compensate for dying MNs. Most of our current knowledge about surviving spinal

MNs in ALS mouse models has largely been generated by gene expression profiling of both whole spine and micro-dissected tissue and cells [41,21,13,6,20,59]. However, these studies provide just a single snapshot of the MN's biology and only allow for inferences to be made about how changes in gene expression alter MN physiology, allow them to resist degeneration, or compensate for dying neurons by forming new motor endplate attachments. In the current study, we sought to functionally characterize ALS-resistant MNs by culturing them *in vitro*, where we would be able to directly assess dynamic cellular properties such as outgrowth, branching, and regulation of the cytoskeleton. We found that in comparison to age-matched, non-transgenic controls, motor neurons cultured from G93A mouse models have enhanced axonal outgrowth and dendritic outgrowth/branching. They also have an increase in both number and size of actin-based cell structures such as growth cones and filopodia. Interestingly, increased outgrowth capacity is correlated with disease progression. This phenotype occurs independently of SOD1 enzymatic activity and is cell autonomous. Further, the enhanced outgrowth occurs before the mice become symptomatic, though the effect does increase with disease progression. These results indicate that the surviving motor neurons in ALS are primed for regeneration, well before an individual gets sick, in response to cellular stress. Identifying the signaling pathways and functional mechanisms involved in this regenerative response could open up novel avenues for experimental treatments for ALS patients.

Materials and Methods

Mouse colony housing and breeding

All studies involving mice were approved by the Institutional Animal Care and Use Committee (IACUC) at the University of Florida in accordance with NIH guidelines. Adult mice were housed one to five per cage and maintained on ad libitum food and water, with a 12 h light/dark cycle. Transgenic mouse strains SOD1-G93A and SOD1-G93Adl (JAX stock #004435 and #002299 respectively [30] were purchased from Jackson laboratory (Bar Harbor, Maine), and bred by the Rodent Breeding Services offered by the Animal Care Services at the University of Florida. SOD1-G93A and SOD1-G93dl colonies were maintained by breeding hemizygous mice either to wild type siblings, or to C57BL/6J inbred mice (Jax Stock # 000664). Additional transgenic mice strains used in this study were G85R-SOD1:YFP, previously described by [70] and WT-SOD1 (JAX stock #002297), both strains were generously supplied by Dr. Borchelt. The G85R-SOD1:YFP mice were maintained as heterozygotes on the FVB/NJ background and whereas the WT-SOD1 were maintained on a C57Bl/6J and C3H/HeJ hybrid background. For the studies involving G85R-SOD1:YFP mice which were induced to develop ALS, please refer to a full description of the procedure by Ayer *et al* [5].In addition to the adult mice, we also used timed-pregnant C57BL/6J and SOD1-G93dl mice at gestational day 14, which were also generated by the Rodent Breeding Services offered by the Animal Care Services at the University of Florida.

Colony maintenance genotyping for all strains was performed as previously described [30,69]. Furthermore, to control for possible transgene copy loss due to meiotic rearrangement, breeders were regularly screened by RT-PCR as previously described [32] and replaced with fresh founder stocks from Jackson laboratory (Bar Harbor, Maine) every 5 generations. In our colony SOD1-G93A and SOD1-G93dl mice reached late disease stage at 150-180 days and 240-330 days of age respectively.

Assessment of ALS disease progression

Mice were considered symptomatic if they displayed a 15% loss of bodyweight or showed signs of leg paralysis, whichever was reached first. In our hands, the majority of mice (~70%) were euthanized because of leg paralysis, and the rest due to decreased body weight. All mice were euthanized by CO2 inhalation following the guidelines provided by the University of Florida Animal Care Services (ACS) and approved by the Institutional Animal Care and Use Committee (IACUC).

Study design

To control for gender differences in disease progression and phenotype of SOD1-G93A mice, symptomatic adult G93A and G93A DL mice were always paired with NTg mice of the same gender and of similar age for each experiment, in most cases using littermates. Age and gender matching also allowed us to control for batch differences in the conditioned medium used to culture adult MN as described below under “cell culture conditions”.

Adult and embryonic mouse spinal cord isolation

Embryo spinal cords were obtained from timed pregnant G93ADL and C57BL/6J mice at embryonic day 14 as previously described in detail [7]. Once embryos were removed from the uterus, spinal cords were extracted under sterile conditions in a laminar flow hood with the aid of a dissecting

microscope (SMZ800, NIKON INSTRUMENTS INC.) and small forceps and placed into cold Leibovitz's L-15 medium (Life Technologies, Grand Island, NY) supplemented with 25 µg ml^{-1} penicillin-streptomycin (Life Technologies). The meninges and dorsal root ganglia (DRG) were peeled off and individual spinal cords were transferred into a 12 wells plate, identified and kept in cold L-15 medium on ice. Tails from each embryo were also harvested at this point for genotyping (G93A-DL mice).

Adult spinal cords were isolated by cutting the vertebrate column with scissors in front of the back legs and just below the medulla oblongata and flushed out of the spinal column using a syringe filled with cold supplemented DMEM/F12-medium with 18G needle (BD Biosciences). The DMEM/F12-medium used for this purpose consisted of DMEM/F12 in a 3:1 ratio supplemented with 36.54 mM NaHCO3 (Fisher Scientific), 0.18 mM L-adenine (Sigma), 312.5 µl L^{-1} 2N HCL (Fisher Scientific), 10% of fetal calf serum (Hyclone, GE Healthcare Life Sciences, South Logan, Utah) and 25 µg ml^{-1} of penicillin-streptomycin (Life Technologies). The adult spinal cords were transferred into cold DMEM/F12-medium.

MN cell extraction and separation

Both embryonic and adult motor neurons were extracted using the method and reagents described in detail by Beaudet et al. [7] with a few modifications. Briefly, individual spinal cords were cut into small pieces and incubated for 30 min at 37C in digestion buffer consisting of Dulbecco's PBS (DPBS, Life Technologies, Grand Island, NY) containing 10 U/ml^{-1} papain (Worthington, Lakewood, NJ, USA), 200ug/ml^{-1} L-cysteine (Sigma St. Louis, MO) and 250 U/ml^{-1} DNase (Sigma, St. Louis, MO). The digestion buffer was then removed and replaced with DPBS containing 8 mg/ml Ovomucoid trypsin inhibitor (Sigma), 8 mg/ml bovine serum albumin (BSA, Sigma), and 250 U/ml DNase. The tissue was then triturated using glass pipettes to obtain a single-cell suspension This step was repeated trice before all cells were collected and filtered through a 40 µm cell strainer (BD Falcon) and centrifuged at 280 g for 10 min at 4 °C for MN. Adult mixed motor neuron cultures were ready to plate after this step. Embryonic MN pellets were enriched by resuspending in 6 ml of cold Leibovitz's L-15 medium (Life Technologies) and laid over a 1.06 g ml−1 Nycoprep density solution (Axis-Shield, Dundee, Scotland) and spun at 900 g for 20 min at 4 °C without brake in a swinging bucket centrifuge (Eppendorf, Hauppauge, NY). MN were collected at the interface of the Nycoprep solution and poured in a new 50 ml collection tube which was then filled with cold L-15. MN cells were counted at this step. MN collecting tubes were centrifuged at 425 g for 10 min in a swinging bucket centrifuge at 4 °C.

Cell culture

Embryonic MN pellets were gently resuspended at 200,000 cells/cm^2 in freshly prepared Motor Neuron Growth Medium (MNGM), which is described in detail by Graber DJ *et al* [27]. Briefly, the MNGM consists of Neurobasal A medium (NB-medium, Life Technologies) supplemented with 1X B-27 Serum-Free Supplement (Gibco/Life Technologies), 1X SATO supplement, 5 µg mL^{-1} Insulin (Gibco/Life Technologies), 1 mM Sodium pyruvate (Gibco/Life Technologies), 2 mM L-Glutamine (Gibco/Life Technologies), 40 ng mL^{-1} of 3,3,5-triiodo-L-thyronine sodium salt (T3; Sigma-Aldrich), 1 µg mL^{-1} Mouse laminin (Gibco/Life Technologies), 417 ng mL^{-1} Forskolin (Sigma-Aldrich), 5 µg mL^{-1} N-acetyl-L-cysteine (NAC, Sigma-Aldrich) and 1x Penicillin-streptomycin (Gibco/Life Technologies).

After filter-sterilization using a 22um syringe filter, 10 ng mL^{-1} of each of the following growth factors was added to the medium: brain-derived neurotrophic factor (BDNF; Sigma-Aldrich), ciliary neurotrophic factor (CNTF; Peprotech, Rocky Hill, NJ) and glial-derived neurotrophic factor (GDNF; Peprotech). Embryonic MNs were either seeded on to Poly-D-lysine coated 6cm tissue culture plates (10 µg mL^{-1}poly-D-lysine, PDL, Sigma-Aldrich) to generate conditioned medium used for adult MN cultures, or on to 1.5 cm glass coverslips pre-coated first with PDL (10 µg mL^{-1} for 1h at RT) then with Human Placental Laminin for 3 h at 37ºC (1.67 µg mL^{-1} laminin in NB-Medium, Sigma-Aldrich). Embryonic motor neurons grown on coverslips were cultured for 3 days prior to fixation in 4% PFA and immunostaining for imaging and growth analysis.

Adult mixed motor neuron cultures were seeded onto PDL coated cover slips (10 µg $mL^{-1)}$ and cultured in MNGM which had been pre-conditioned for 4 days by embryonic motor neurons isolated from WT C57BL/6J mice. Given that adult MN pallets contain considerable amount of debris when first plated, cells were not counted prior to seeding. After the cells were allowed to attach to the coverslips in a humidified 37ºC incubator for 1 h, they were washed twice with warm NB-medium to remove debris and cultured in 1 ml of conditioned MNGM mixed 1:1 with freshly prepared MNGM. Adult MNs were cultured for 2 days prior to fixation and immunostaining for imaging and growth analysis. MN's where selected for analysis based on their expression of Tuj1, their large size, multi-polarity and soma shape.

Immunofluorescence

Cells were fixed with 4% electron microscopy grade paraformaldehyde (PFA, Electron Microscopy Sciences, Hatfield, PA) for 10 min at RT, permeabilized with 0.2% Triton X-100 (Sigma-Aldrich) for 3 min, and washed twice with 1X DPBS. Cells were stained overnight at 4ºC with primary antibodies diluted in immunofluorescence staining buffer. They were then washed twice with DPBS for 5 min, incubated with secondary antibodies (diluted 1:1000) for 1 hr at room temperature in immunofluorescence staining buffer. F-actin was stained with Phalloidin-568 (diluted 1:100, Life Technologies) for 30 min at room temperature in immunofluorescence staining buffer. Finally, cells were washed three times with DPBS before mounting with Prolong Diamond W/ DAPI (Life Technologies). We used the following antibodies/stains: Mouse anti-beta3 Tubulin (TUJ1 1:500 dilution, Covance, Princeton, NJ), Goat anti-ChAT (1:1000, AB144, ED Millipore), mouse anti-Tau (1:25000, gifted from the Giasson lab [61]) Alexa Fluor™ Phalloidin 568, anti-mouse IgG 488 and anti-rabbit IgG 488 (Life Technologies) used at 1:1000.

Imaging

Imaging of IF stained motor neurons was performed on a Nikon A1R+ laser scanning confocal microscope with 40X 1.3 NA and 60X 1.49 NA objectives and the GaAsP multi-detector unit. Imaging of cells for outgrowth and branching pattern analysis was done using the EVOS XL digital inverted microscope (Life Technologies).

Image analysis

Neurite growth cone analysis: Confocal z-stacks were converted into a single maximum intensity projection image. Terminal neurite growth cone size, filopodia length, and filopodia number were

analyzed using Fiji (ImageJ) software. Filopodia length was defined as the distance between lamellipodium edge to the furthest end of the extending filopodia. Values were exported into Microsoft Excel and Graphpad Prism for statistical analysis.

Neurite tracing and branching analysis: Images were taken on the EVOS XL digital inverted were imported into Fiji (ImageJ) software. All visible projections in these images were traced using the Simple Neurite Tracer plugin [42]. An image stack was created from the tracing which was then analyzed using the Sholl analysis plugin [23]. To compare the relative change in neuron radius between wild type and SOD1 mutants across different experiments each set was normalized to the average radius of the age matched wild type control group. The Sholl profile containing the number of branches per given distance from soma and overall neuron radius was then exported to Microsoft Excel or Graphpad Prism for analysis.

Axon tracing and analysis

Staining of motor neuron cultures were performed as previously described with mouse-anti Tau antibody. Imaging was performed on the EVOS XL digital inverted microscope and images were imported into Fiji (ImageJ) software. The 16 bit color lookup table was applied to each image to visualize the intensity of Tau-staining in the neurites. The neurite that was most intensely stained for Tau was then measured from the center of the soma to determine if it was longest projection from the cell.

Statistics

For comparison of multiple data sets paired student's t-tests were used assuming a two-tailed distribution. Significance is indicated on all of the figures and the error bars on all graphs indicate the 95% confidence intervals for each data set. P-values were obtained ANOVA followed by Tukey's post-hoc test.

Results and Discussion

ALS-resistant G93A motor neurons have enhanced neurite outgrowth

Using a well characterized protocol for adult motor neuron extraction [7], we isolated MNs from whole spinal cords from SOD1^{G93A} high copy number mice (referred to as G93A) at late disease stage (defined by hind leg paralysis/weight loss), occurring between postnatal days 150 and 180. Cells were cultured for two days *in vitro* and immunostained for β3 tubulin (Tuj1) and Choline Acetyltransferase (ChAT) to confirm our success in isolating MNs (Supplemental Fig. 1) as described by others [7]. For imaging and analysis purposes, we stained the cells with Tuj1 and phalloidin (for actin visualization) and selected MNs based on their large soma size, multi-polarity and Tuj1 positive staining. Importantly, MN cultures from ALS mouse models were always made in parallel with MN cultures from a sex- and age-matched, none transgenic littermates (NTg) to control for experimental variability. During cell isolation, all established neuronal projections are severed, thus this assay is a direct measurement of the cells' ability to generate new processes. We performed a large-scale quantitative analysis of MN size and branching complexity by tracing the neurons and performing Scholl analysis. Interestingly, MNs from G93A mice displayed substantially increased outgrowth in comparison to NTg MNs, both in neurite length (~40% longer than NTg cells) and number of branches per cell (Fig. 1a-d). While it is known that ALS-resistant MNs have altered RNA expression profiles, including some genes involved in cytoskeletal pathways, the genetic changes observed are usually associated with the negative regulation of outgrowth [53]. Hence, we were surprised to discover that ALS-resistant MNs actually have an enhanced capacity for outgrowth following neurite severing.

While the G93A mouse is the most extensively studied rodent model of ALS, there is some concern about its use given that such a high copy number of the transgene is required to generate the rapid onset of ALS symptoms. This is in contrast to human SOD1-based ALS, where individuals expressing 1 copy of mutant SOD1 at endogenous levels can develop the disease. To determine if the enhanced outgrowth of G93A MNs could occur with a more physiologically relevant level of expression, we cultured cells from another mouse model, SOD1^{G93A}-DL (referred to as G93A-DL), which only has 6-8 transgene copies per cell, hence referred to as dilute (DL) [1]. These mice still get ALS, but disease progression is slower, with a delayed end-stage occurring when the mice are between 8-11 months of age. Surprisingly, MNs isolated from end-stage G93A-DL mice exhibited an even greater outgrowth capacity over age-matched NTg MNs than that observed for the G93A MNs. Compared to controls, G93A-DL exhibit a ~55% median outgrowth length increase (Fig.1f, g) and had more than twice the number of branches >40 μm away from the cell body (Fig. 1f, h), with a continuous increase to more than 3 times as many branches at 70μm away from the cell body (Fig.1f). Thus, in diseased animals expressing SOD1 G93A at more clinically relevant levels, there is an innate program of enhanced neurite outgrowth, which may actually be attenuated by increased amounts of mutant SOD1.

To further investigate whether the increased outgrowth of neurites also meant an increase in axonal regeneration, we stained the cells with anti-Tau to distinguish axons from dendrites. Based on having the highest Tau fluorescence intensity, we determined that 63% of the cells analyzed had a process that could be identified as the axon. Of these cells, the neurite with the highest Tau fluorescence was also the longest process 79% of the time (Supplemental Fig. 2). This implies that, in addition to the

observed increase in dendritic arborization as defined by the number of processes, the enhanced increase in overall cell radius corresponds to increased axonal regenerative capability.

The G93A mutation preserves the enzymatic activity of SOD1, which is to remove superoxide radicals. Reactive oxygen species (ROS) such as superoxide ($O2^-$), hydrogen peroxide (H_2O_2) and the hydroxyl radical (OH^-) are used by neurons in intracellular signaling events during apoptosis, differentiation, and cell migration [45,64]. Hence, a potential explanation for the enhanced outgrowth seen in ALS-resistant MNs from G93A and G93A-DL mice might be that rather than a survival response to cell stress, the overexpression of mutant SOD1 alters redox signaling in a manner that promotes formation and extension of neurites. We tested this possibility by culturing MNs from heterozygote mice overexpressing wild-type human SOD1 (referred to as WT-SOD1). Importantly, heterozygote WT-SOD1 mice do not get ALS [24,28], which reduces the possibility of an activated MN stress response in these mice. Relative to age-matched NTg control MNs, WT-SOD1 MNs actually exhibited a slight decrease in outgrowth and branching (Fig. 1i-l) (p-value= 0.002 and 0.03, respectively). This is consistent with previous findings where ROS depletion in neurons has been shown to have negative effects on neurite outgrowth [48]. Therefore, it is unlikely that the enhanced outgrowth of G93A MNs is attributed to increasing the level of enzymatically active SOD1.

Another potential explanation for the enhanced outgrowth phenomenon we observed is that ALS-resistant G93A cells grow bigger because they are actually larger cells to begin with. This notion is contradictory to published *in vivo* studies of spinal cord tissue from patients and mouse models with ALS, where surviving MNs have significantly reduced soma size due to the small γ fusimotor neurons (γ-MNs) being selectively disease resistant [39]. However, since no previous studies have characterized the size of cultured ALS-resistant MNs, we sought to determine if the cells that generate the longest neurites were also the largest cells. We measured the soma of NTg, G93A, and G93A-DL MNs to determine if neurite growth correlated with the size of the cell body. While the mean soma area did increase significantly in G93A and G93A-DL MNs compared to NTg cells, we found that within each group, soma area was not correlated with neurite length and could therefore not be used to predict outgrowth (Suppl. Fig. 1). Thus, cell size is not a potential explanation for the increased outgrowth and branching phenotype seen in G93A and G93A-DL MNs.

Mutant SOD1 MNs acquire enhanced ability to regenerate before onset of ALS symptoms

Having established that end-stage ALS-resistant MNs from both G93A and G93A-DL mouse models have an enhanced capacity for neurite outgrowth and branching, we next wanted to determine if this was a survival response to ALS-induced cell death or if the neurons acquired this phenotype earlier in the disease process. To do so, we first cultured MNs from asymptomatic G93A-DL mice at two and six months of age, and from 2-month-old G93A mice and measured the outgrowth and branching. We found that G93A-DL MNs from both age groups exhibited increased outgrowth compared to NTg cells (Fig. 2a-c), whereas MNs from 2-month-old G93A mice did not display any enhanced outgrowth capacity (Fig. 2d-f). Furthermore, we found that at 40 μm from the soma, only the 6-month-old-mice G93A-DL mice displayed increased branching compared to NTg controls (Fig. 2b). When compared to the nine-month-old symptomatic G93A-DL mice, a clear trend was evident where branching of the

cultured MNs increased with age and disease progression, whereas no such increased branching was seen in the G93A MNs at 2 months of age. It is interesting that a pre-symptomatic phenotype was only seen in cells expressing low amounts of G93A, though perhaps this may reflect a difference in how the disease develops between the two mouse models: sudden onset with rapid progression for the G93A mouse and slower, more gradual progression of symptoms for the G93A-DL mouse. Alternatively, this might reflect a concentration response, where low levels of SOD1 G93A at any postnatal stage renders enhanced outgrowth, whereas high levels do not.

To further confirm that the enhanced outgrowth of ALS-resistant MNs is not triggered by disease onset, we cultured cells from heterozygous mice overexpressing SOD1^{G85R} fused with yellow fluorescent protein (YFP) (referred to simply as G85R mice). G85R is another well-documented mutant of SOD1 where mice homozygote for G85R develop ALS, whereas the heterozygote mice never become symptomatic [68]. Hence, this is a useful model for studying the effects of the mutation at low dosage in the absence of disease onset. Surprisingly we found that G85R MNs cultured from 6-month-old mice displayed a similar increase in branching and outgrowth as MNs from G93A mouse models, although the branching pattern was somewhat different, with the most significant differences (double the number of branches) occurring between 50-80 μm from the soma (Fig. 2g-i). Given that the heterozygote G85R mice do not develop ALS, the motor neurons extracted from these mice have not been subjected to selection through disease resistance and thus represent all adult MNs with SOD1 mutations, not just those resistant to ALS. Thus, the enhanced outgrowth phenotype is not induced by the onset of ALS. To determine if this inherent outgrowth phenotype would be further enhanced with ALS disease onset, we extracted MNs from adult G85R mice that had been injected with mutant SOD1 fibrils, which has been previously reported to induce ALS in these mice [5]. Interestingly, we found that these ALS-resistant MNs were twice as big and had twice as many branches at 40 μm from the soma compared to the un-induced G85R MNs (Fig. 2g-i). Furthermore, ALS-resistant MNs from induced G85R mice were 30-40% longer and more branched compared to NTg controls than end-stage G93A-DL MNs (Fig. 1e-h). This demonstrates that mutant SOD1 expression by itself induces enhanced MN outgrowth and that upon induction and progression of ALS, this phenotype is further enhanced in disease resistant MNs. It is also of note than unlike G93A, the G85R mutant loses most of its enzymatic activity [12,16], further confirming that the enhanced outgrowth seen in mutant SOD1 MNs is not due to altered redox signaling resulting from SOD1 enzymatic activity.

Having established that adult MNs from multiple backgrounds exhibited an enhanced outgrowth independent of ALS onset, we then sought to determine if this phenotype was innate to MNs expressing mutant SOD1 by culturing embryonic MNS. We isolated MNs from individual G93A-DL and NTg pups at E14 and measured outgrowth after 3 days in culture. No significant difference was observed in outgrowth or branching compared to NTg controls (Fig. 2j-l). Thus, the enhanced outgrowth phenotype appears to be acquired in early in adulthood, rather than exist as an inherent trait of MNs expressing low levels of mutant SOD1. This result also underscores the importance of using adult MN cultures for functional characterization of cells during disease progression.

Enhanced outgrowth of ALS-resistant MNs is cell autonomous

There is considerable evidence showing that the SOD1 mutant-mediated ALS disease process is both cell and non-cell autonomous [18,10,72,70]. While synthesis of mutant SOD1 within motor neurons is a primary driver of the disease, expression of mutant SOD1 by other cells such as interneurons, microglia, astrocytes, Schwan cells and T-lymphocytes substantially contribute to the progression of ALS [10,8,26,72,40,9,17]. Given that our MN cultures are not entirely free from contaminating cells such as microglia and astrocytes, it is possible that non-neuronal cells were present in different ratios in NTg vs. mutant SOD1 cultures and/or are differentially secreting factors that contribute to the increased outgrowth seen in G93A, G93A-DL, and G85R MNs. To test this possibility, we harvested conditioned medium from 3-day-old G93A, G93A-DL, and NTg adult MN cultures and used this medium to culture NTg MNs to see if it could influence neurite out growth. While conditioned media from G93A and G93A-DL MNs did slightly increase outgrowth of NTg MNs, the median difference was only ~5% (Fig. 3 a-c) increase, or roughly 10-20 times less than the median outgrowth differences of G93A, G93A-DL, (Fig. 1a-h), or G85R MNs (Fig. 2g-i) relative to their NTg controls. These data suggest that the observed enhanced outgrowth and branching phenotype of ALS-resistant MNs is not a result of secreted factors from non-neuronal cells, but rather an intrinsic quality of these MNs.

ALS-resistant MNs have increased growth cone size, number, and filopodia length

Previous studies have implicated that SOD1 mutations may be linked to cytoskeletal defects in MNs vulnerable to ALS [46,71]. Furthermore, G93A has been shown to bind actin and negatively disrupt the actin cytoskeleton [63]. However, enhanced branching and neurite extension are usually associated with actin-based structures, such as the growth cone's lamellipodia and filopodia, which are positive regulators of neurite outgrowth. To investigate whether ALS resistant G93A MNs displayed abnormalities in their actin cytoskeleton, we co-stained end-stage cells for filamentous actin (F-actin) and Tuj-1. Surprisingly, ALS-resistant MNs from G93A and G93A-DL mice had larger growth cones than NTg MNs (Fig. 4a-c) and approximately double the amount of growth cones per cell (Fig. 4d). We also found that there was twice as many filopodia per growth cone and the filopodia were 50% longer in ALS-resistant MNs (Fig. 4e, f). Interestingly, this actin phenotype was not present MNs from asymptomatic 2- or 6-month-old mice (Fig. 4g-h), suggesting that as a late-stage adaptation response, MN's upregulate actin-based processes that favor the formation of structures that enhance outgrowth and regeneration.

As mentioned previously, there are several published studies characterizing genetic changes in MNs from G93A mice at various stages of disease progression [53,21,51,19,29,58,20,73]. However, these studies have not reached consensus regarding the underlying genetics promoting ALS resistance, probably due to the variation in experimental design and tissue sampling. For example, using G93A mice, one study found a massive up-regulation of genes involved in cell growth and/or maintenance from micro-dissected motor neurons from the lumbar spinal cord [53], whereas another study found Wnt signaling to be significantly activated when homogenized whole spinal cord was used for RNA extraction [73]. Apart from a single study showing SOD1 binding of actin [63], little is known about

actin dynamics in SOD1 driven ALS, although it has been shown that upregulation of axonal guidance genes and actin cytoskeletal genes (including alpha- and beta-actin) occurs from the lumbar spinal cord of pre-symptomatic G93A mouse [20]. This could explain our results showing that well before symptoms become present, G93A MNs are actually primed for outgrowth and regeneration, at least in part due to a positive activation of the actin cytoskeleton. It is also worth noting that Lobsiger *et al.* found that regenerative/injury pathways genes were upregulated both in dismutase active and inactive (G37R and G85R) MNs at disease onset, including ATF3, a gene also known to be upregulated in end stage in G93A mice [41,56,66,11,67]. While it has been speculated that upregulation of regenerative/injury pathways is merely a compensatory response to mutant SOD1G93A-dependent impairment of axonal regeneration [41,55] we don't believe this explains the enhanced outgrowth of ALS-resistant MNs since even heterozygote G85R-SOD1:YFP mice, which never develop ALS and therefore do not experience SOD1 mutant dependent MN degeneration, still exhibit the phenotype. Further studies are needed to determine if the enhanced outgrowth seen in ALS resistant MNs is due to transcriptional regulation of actin cytoskeletal proteins and if so which stress signals induce this response in early pre-symptomatic stages.

Acknowledgments

This project was supported by a Pathway to Independence Award from the National Institutes of Health (R00 NS087104) to E.A.V.

Figure Legends

Figure 1. G93A and G93A-DL motor neurons from ALS symptomatic mice exhibit an increased outgrowth phenotype. (a) Representative images of motor neurons harvested from symptomatic SOD1-G93A transgenic mice (G93A) and age-matched, non-transgenic (NTg) controls (top) and the same images after tracing and Sholl analysis, color coded to show the number of intersections at various length intervals from the soma (bottom). **(b)** A Sholl graph, representing the average number of neurite branches per distance from the soma, of G93A MNs from symptomatic mice and age-matched NTg controls. **(c)** Box-and-whisker plot of the relative outgrowth (measured as the length of the longest neurite branch) of G93A MNs from symptomatic mice relative to their age-matched NTg controls. **(d)** Box-and-whisker plot of number of intersections present 40 μm (indicated by dotted line in (b) from the soma for G93A MNs from symptomatic mice and NTg controls. For (b), (c), and (d) n=88 from 4 mice and n=120 from 5 mice for NTg and G93A data sets, respectively. **(e)** Representative images (top) and results of Sholl analysis (bottom) of motor neurons harvested from age-matched NTg and symptomatic G93A-DL transgenic mice, demonstrating a pronounced increase in outgrowth and branching of the G93A-DL MNs. **(f)** Sholl graph of G93A-DL MNs from symptomatic mice and age-matched NTg controls. **(g)** Box-and-whisker plot showing the relative increase in outgrowth between NTg controls and G93A-DL MNs from symptomatic mice. **(h)** Box-and-whisker plot showing number of branches 40 μm from the soma for NTg controls and G93A-DL MNs from symptomatic mice. For (f), (g), and (h) n=56 from 3 NTG mice and n=62 from 3 G93A-DL mice. **(i)** Representative images of $SOD1^{WT}$ transgenic mice and their age-matched NTg controls. **(j)** Sholl graph of $SOD1^{WT}$ transgenic mice and their age-matched NTg controls, showing a slight decrease in

branching at 40 μm from the soma. **(k)** Box-and-whisker plot of the relative outgrowth between NTg and $SOD1^{WT}$ motor neurons, again a small but significant decrease in outgrowth. **(l)** Box-and-whisker plot showing number of branches 40 μm from the soma for NTg and $SOD1^{WT}$ transgenic MNs. For (j), (k), and (l) n=82 from 2 mice and n=89 from 3 mice, for NTg and $SOD1^{WT}$, respectively. Error bars on Sholl graphs are 95% confidence intervals. Box-and-whisker plots denote the 95th (top whisker), 75th (top edge of box), 25th (bottom edge of box), and 5th (bottom whisker) percentiles, and the median (bold line in box). Each point on the graph represents an individual cell measurement, scattered with random noise in the x direction to enable visualization of all points for the given data set. p-values were obtained from a two-tailed student's T-test. The image scale bars are 100 μm.

Figure 2. The increased outgrowth phenotype in SOD1-G93A-DL motor neurons can be observed before onset of ALS symptoms. (a) Representative images of G93A-DL MNs from presymptomatic mice at both 2, 6, and 9 months of age and their age- and gender-matched NTg controls showing a relative increase in outgrowth in G93A-DL MNs presymptomatic mice at 2, 6, and 9 months. **(b)** Line graph representing the fold change in radius between G93A-DL MNs and their age and sex matched NTg counterparts at 2, 6, and 9 months. For (b) and the data set taken at 2 months n=95 for NTg and n=80 for G93A-DL, harvested from 3 mice each. The data set representing 6 months was taken from 3 mice each for NTg and G93A-DL, with n=88 and n=80 respectively. The data set representing 9 months was taken from 3 NTG mice and 3 G93A-DL mice, with n=56 and n=62 respectively. **(c)** Representative images of G93A MNs from 2-month-old presymptomatic mice and their age- and gender-matched NTg controls. **(d)** Sholl graph of G93A MNs from 2-month-old presymptomatic mice and their age-matched NTg controls showing a similar amount of branching and outgrowth between the two. **(e)** Box-and-whisker plot showing relative outgrowth of G93A MNs from 2-month-old presymptomatic mice and their age-matched NTg controls. For (d) and (e) n=60 harvested from 3 mice for NTg and n=60 harvested from 3 mice for G93A. **(f)** Representative images of MNs from heterozygous, 9-month-old G85R transgenic mice, MNs from symptomatic G85R transgenic mice induced to get ALS by injecting spinal cord homogenate from another ALS-symptomatic mouse, and an age- and gender-matched NTg control. **(g)** Sholl graph of MNs from G85R transgenic mice (asymptomatic 9-month-old and symptomatic induced) and their age-matched NTg controls. G85R MNs exhibit increases in outgrowth and branching relative to NTg controls, but this effect is significantly enhanced when the mice are induced to get ALS. **(h)** Box-and-whisker plot showing the relative outgrowth of MNs from G85R transgenic mice (asymptomatic 9-month-old and symptomatic induced) and their age-matched NTg controls. For (g) and (h) n=23 from 2 mice for NTg and n=51 from 4 mice for G85R, n=50 from 2 mice for G85R induced. **(i)** Representative images of E14 NTg and G93A-DL motor neurons, showing the similarity in branching and outgrowth. **(j)** Sholl graph of E14 NTg and G93A-DL motor neurons. **(k)** Box-and-whisker plot depicting relative outgrowth of E14 NTg and G93A-DL motor neurons. For (j) and (k) n=26 and n=17 for NTg and G93A-DL, each harvested from 2 mice. Error bars on Sholl graphs are 95% confidence intervals. Box-and-whisker plots denote the 95th (top whisker), 75th (top edge of box), 25th (bottom edge of box), and 5th (bottom whisker) percentiles, and the median (bold line in box). Each point on the graph represents an individual cell measurement, scattered with random noise in the x direction to enable visualization of all points for the given data set. p-values were obtained from a two-tailed student's T-test (2

conditions) or ANOVA followed by Tukey's post-hoc test (3-4 conditions). The image scale bars are 100 μm.

Figure 3. Culturing non-transgenic motor neurons in media conditioned by G93A and G93A-DL motor neurons does not recapitulate outgrowth phenotype. (a) Representative images of MNs harvested from NTg mice, cultured in medium conditioned (CM) by NTg, G93A, or G93A-DL motor neurons. **(b)** Sholl graph of MNs harvested from NTg mice, cultured in media conditioned by NTg, G93A, or G93A-DL motor neurons, depicting overlapping confidence intervals for all three conditions at all distances from the soma. **(c)** Box-and-whisker plot relative outgrowth of MNs harvested from NTg mice, cultured in medium conditioned by NTg, G93A, or G93A-DL motor neurons, showing a slight but statistically significant increase in outgrowth when NTg MNs are cultured in media conditioned by G93A or G93A-DL cultures. For (b) and (c) n=138 from 3 mice for NTg/NTg-CM, n=134 from 3 mice for NTg/G93A-CM, and n=60 from 2 mice for NTg/G93A-DL-CM. Error bars on Sholl graphs are 95% confidence intervals. Box-and-whisker plots denote the 95th (top whisker), 75th (top edge of box), 25th (bottom edge of box), and 5th (bottom whisker) percentiles, and the median (bold line in box). Each point on the graph represents an individual cell measurement, scattered with random noise in the x direction to enable visualization of all points for the given data set. p-values were obtained ANOVA followed by Tukey's post-hoc test. The image scale bars are 100 μm.

Figure 4. Growth cones and filopodia are larger and more numerous in G93A and G93A-DL motor neurons from symptomatic mice. (a) Representative images from motor neurons cultured from NTg, G93A-DL, and G93A mice demonstrating the increase in overall neuron radius, as well as the increase in number of growth cones. Image scale bars are 20 μm **(b)** A magnified look at growth cones from motor neurons cultured from NTg, G93A-DL, and G93A mice, showing the increase in growth cone area, filopodia length, and filopodia per growth cone in G93A and G93A-DL MNs. Image scale bar is 5 μm. **(c)** Box-and-whisker plot depicting growth cone area for MNs cultured from NTg, and G93A-DL mice. **(d)** Box-and-whisker plot depicting number of growth cones per motor neuron for MNs cultured from NTg, and G93A-DL mice. **(e)** Box-and-whisker plot depicting the number of filopodia per growth cone for MNs cultured from NTg, and G93A-DL mice. **(f)** Box-and-whisker plot depicting filopodia length for MNs cultured from NTg, and G93A-DL mice. For (c-f) n=25 for NTg, and n=25 for G93A-DL, harvested from two mice for each. **(g)** Line graph representing the fold change in growth cone area between G93A-DL and their NTg controls, normalized to the NTg control for each condition. **(h)** Line graph representing the fold change in filopodia length between NTg and G93A-DL cells, represented as described in (g). For (g) and (h) 2 NTg and 2 G93A-DL mice were analyzed at each time point. At 2 months n=18 cells for NTg and n=32 cells for G93A-DL. At 6 months n=20 cells for NTg and n=19 cells for G93A-DL. **(i)** Box-and-whisker plot depicting the growth cone area for MNs cultured from NTg and symptomatic G93A mice. **(j)** Box-and-whisker plot depicting filopodia length for MNs cultured from NTg and G93A mice. For (i) and (j) n=38 cells for NTg and n=28 cells for G93A, harvested from 2 mice each. Box-and-whisker plots denote the 95th (top whisker), 75th (top edge of box), 25th (bottom edge of box), and 5th (bottom whisker) percentiles, and the median (bold line in box). Each point on the graph represents an individual cell measurement, scattered with random

noise in the x direction to enable visualization of all points for the given data set. p-values were obtained from a two-tailed student's T-test.

References

1. Acevedo-Arozena A, Kalmar B, Essa S, Ricketts T, Joyce P, Kent R, Rowe C, Parker A, Gray A, Hafezparast M, Thorpe JR, Greensmith L, Fisher EM (2011) A comprehensive assessment of the SOD1G93A low-copy transgenic mouse, which models human amyotrophic lateral sclerosis. Dis Model Mech 4:686-700. doi:10.1242/dmm.007237

2. Achilli F, Boyle S, Kieran D, Chia R, Hafezparast M, Martin JE, Schiavo G, Greensmith L, Bickmore W, Fisher EM (2005) The SOD1 transgene in the G93A mouse model of amyotrophic lateral sclerosis lies on distal mouse chromosome 12. Amyotroph Lateral Scler Other Motor Neuron Disord 6:111-114. doi:10.1080/14660820510035351

3. Allodi I, Comley L, Nichterwitz S, Nizzardo M, Simone C, Benitez JA, Cao M, Corti S, Hedlund E (2016) Differential neuronal vulnerability identifies IGF-2 as a protective factor in ALS. Sci Rep 6:25960. doi:10.1038/srep25960

4. Andersen PM, Al-Chalabi A (2011) Clinical genetics of amyotrophic lateral sclerosis: what do we really know? Nat Rev Neurol 7:603-615. doi:10.1038/nrneurol.2011.150

5. Ayers JI, Fromholt SE, O'Neal VM, Diamond JH, Borchelt DR (2016) Prion-like propagation of mutant SOD1 misfolding and motor neuron disease spread along neuroanatomical pathways. Acta Neuropathol 131:103-114. doi:10.1007/s00401-015-1514-0

6. Bandyopadhyay U, Cotney J, Nagy M, Oh S, Leng J, Mahajan M, Mane S, Fenton WA, Noonan JP, Horwich AL (2013) RNA-Seq profiling of spinal cord motor neurons from a presymptomatic SOD1 ALS mouse. PLoS One 8:e53575. doi:10.1371/journal.pone.0053575

7. Beaudet MJ, Yang Q, Cadau S, Blais M, Bellenfant S, Gros-Louis F, Berthod F (2015) High yield extraction of pure spinal motor neurons, astrocytes and microglia from single embryo and adult mouse spinal cord. Sci Rep 5:16763. doi:10.1038/srep16763

8. Beers DR, Henkel JS, Xiao Q, Zhao W, Wang J, Yen AA, Siklos L, McKercher SR, Appel SH (2006) Wild-type microglia extend survival in PU.1 knockout mice with familial amyotrophic lateral sclerosis. Proc Natl Acad Sci U S A 103:16021-16026. doi:10.1073/pnas.0607423103

9. Beers DR, Henkel JS, Zhao W, Wang J, Appel SH (2008) CD4+ T cells support glial neuroprotection, slow disease progression, and modify glial morphology in an animal model of inherited ALS. Proc Natl Acad Sci U S A 105:15558-15563. doi:10.1073/pnas.0807419105

10. Boillée S, Yamanaka K, Lobsiger CS, Copeland NG, Jenkins NA, Kassiotis G, Kollias G, Cleveland DW (2006) Onset and progression in inherited ALS determined by motor neurons and microglia. Science 312:1389-1392. doi:10.1126/science.1123511

11. Bonilla IE, Tanabe K, Strittmatter SM (2002) Small proline-rich repeat protein 1A is expressed by axotomized neurons and promotes axonal outgrowth. The Journal of neuroscience : the official journal of the Society for Neuroscience 22:1303-1315

12. Borchelt DR, Lee MK, Slunt HS, Guarnieri M, Xu ZS, Wong PC, Brown RH, Price DL, Sisodia SS, Cleveland DW (1994) Superoxide dismutase 1 with mutations linked to familial amyotrophic lateral sclerosis possesses significant activity. Proc Natl Acad Sci U S A 91:8292-8296

13. Brockington A, Ning K, Heath PR, Wood E, Kirby J, Fusi N, Lawrence N, Wharton SB, Ince PG, Shaw PJ (2013) Unravelling the enigma of selective vulnerability in neurodegeneration: motor neurons resistant to degeneration in ALS show distinct gene expression characteristics and decreased susceptibility to excitotoxicity. Acta Neuropathol 125:95-109. doi:10.1007/s00401-012-1058-5

14. Brown RH, Al-Chalabi A (2017) Amyotrophic Lateral Sclerosis. The New England Journal of Medicine:10

15. Bruijn LI, Becher MW, Lee MK, Anderson KL, Jenkins NA, Copeland NG, Sisodia SS, Rothstein JD, Borchelt DR, Price DL, Cleveland DW (1997) ALS-linked SOD1 mutant G85R mediates damage to astrocytes and promotes rapidly progressive disease with SOD1-containing inclusions. Neuron 18:327-338

16. Cao X, Antonyuk SV, Seetharaman SV, Whitson LJ, Taylor AB, Holloway SP, Strange RW, Doucette PA, Valentine JS, Tiwari A, Hayward LJ, Padua S, Cohlberg JA, Hasnain SS, Hart PJ (2008) Structures of the G85R variant of SOD1 in familial amyotrophic lateral sclerosis. J Biol Chem 283:16169-16177. doi:10.1074/jbc.M801522200

17. Chiu IM, Chen A, Zheng Y, Kosaras B, Tsiftsoglou SA, Vartanian TK, Brown RH, Carroll MC (2008) T lymphocytes potentiate endogenous neuroprotective inflammation in a mouse model of ALS. Proc Natl Acad Sci U S A 105:17913-17918. doi:10.1073/pnas.0804610105

18. Clement AM, Nguyen MD, Roberts EA, Garcia ML, Boillée S, Rule M, McMahon AP, Doucette W, Siwek D, Ferrante RJ, Brown RH, Julien JP, Goldstein LS, Cleveland DW (2003) Wild-type nonneuronal cells extend survival of SOD1 mutant motor neurons in ALS mice. Science 302:113-117. doi:10.1126/science.1086071

19. D'Arrigo A, Colavito D, Peña-Altamira E, Fabris M, Dam M, Contestabile A, Leon A (2010) Transcriptional profiling in the lumbar spinal cord of a mouse model of amyotrophic lateral sclerosis: a role for wild-type superoxide dismutase 1 in sporadic disease? J Mol Neurosci 41:404-415. doi:10.1007/s12031-010-9332-2

20. de Oliveira GP, Alves CJ, Chadi G (2013) Early gene expression changes in spinal cord from SOD1(G93A) Amyotrophic Lateral Sclerosis animal model. Front Cell Neurosci 7:216. doi:10.3389/fncel.2013.00216

21. Ferraiuolo L, Heath PR, Holden H, Kasher P, Kirby J, Shaw PJ (2007) Microarray analysis of the cellular pathways involved in the adaptation to and progression of motor neuron injury in the SOD1 G93A mouse model of familial ALS. The Journal of neuroscience : the official journal of the Society for Neuroscience 27:9201-9219. doi:10.1523/JNEUROSCI.1470-07.2007

22. Ferraiuolo L, Kirby J, Grierson AJ, Sendtner M, Shaw PJ (2011) Molecular pathways of motor neuron injury in amyotrophic lateral sclerosis. Nat Rev Neurol 7:616-630. doi:10.1038/nrneurol.2011.152

23. Ferreira TA, Blackman AV, Oyrer J, Jayabal S, Chung AJ, Watt AJ, Sjöström PJ, van Meyel DJ (2014) Neuronal morphometry directly from bitmap images. Nature methods 11:982-984. doi:10.1038/nmeth.3125

24. Furukawa Y (2012) Pathological roles of wild-type cu, zn-superoxide dismutase in amyotrophic lateral sclerosis. Neurol Res Int 2012:323261. doi:10.1155/2012/323261

25. Gizzi M, DiRocco A, Sivak M, Cohen B (1992) Ocular motor function in motor neuron disease. Neurology 42:1037-1046

26. Gowing G, Philips T, Van Wijmeersch B, Audet JN, Dewil M, Van Den Bosch L, Billiau AD, Robberecht W, Julien JP (2008) Ablation of proliferating microglia does not affect motor neuron degeneration in amyotrophic lateral sclerosis caused by mutant superoxide dismutase. The Journal of neuroscience : the official journal of the Society for Neuroscience 28:10234-10244. doi:10.1523/JNEUROSCI.3494-08.2008

27. Graber DJ, Harris BT (2013) Purification and culture of spinal motor neurons. Cold Spring Harb Protoc 2013:310-311. doi:10.1101/pdb.top070920

28. Graffmo KS, Forsberg K, Bergh J, Birve A, Zetterström P, Andersen PM, Marklund SL, Brännström T (2013) Expression of wild-type human superoxide dismutase-1 in mice causes amyotrophic lateral sclerosis. Hum Mol Genet 22:51-60. doi:10.1093/hmg/dds399

29. Guipponi M, Li QX, Hyde L, Beissbarth T, Smyth GK, Masters CL, Scott HS (2010) SAGE analysis of genes differentially expressed in presymptomatic TgSOD1G93A transgenic mice identified cellular processes involved in early stage of ALS pathology. J Mol Neurosci 41:172-182. doi:10.1007/s12031-009-9317-1

30. Gurney ME (1994) Transgenic-mouse model of amyotrophic lateral sclerosis. N Engl J Med 331:1721-1722. doi:10.1056/NEJM199412223312516

31. Haenggeli C, Kato AC (2002) Differential vulnerability of cranial motoneurons in mouse models with motor neuron degeneration. Neurosci Lett 335:39-43

32. Henriques A, Pitzer C, Schneider A (2010) Characterization of a novel SOD-1(G93A) transgenic mouse line with very decelerated disease development. PLoS One 5:e15445. doi:10.1371/journal.pone.0015445

33. Ilieva HS, Yamanaka K, Malkmus S, Kakinohana O, Yaksh T, Marsala M, Cleveland DW (2008) Mutant dynein (Loa) triggers proprioceptive axon loss that extends survival only in the SOD1 ALS model with highest motor neuron death. Proc Natl Acad Sci U S A 105:12599-12604. doi:10.1073/pnas.0805422105

34. Ince PG, Lowe J, Shaw PJ (1998) Amyotrophic lateral sclerosis: current issues in classification, pathogenesis and molecular pathology. Neuropathol Appl Neurobiol 24:104-117

35. Jonsson PA, Graffmo KS, Brännström T, Nilsson P, Andersen PM, Marklund SL (2006) Motor neuron disease in mice expressing the wild type-like D90A mutant superoxide dismutase-1. J Neuropathol Exp Neurol 65:1126-1136. doi:10.1097/01.jnen.0000248545.36046.3c

36. Kaplan A, Spiller KJ, Towne C, Kanning KC, Choe GT, Geber A, Akay T, Aebischer P, Henderson CE (2014) Neuronal matrix metalloproteinase-9 is a determinant of selective neurodegeneration. Neuron 81:333-348. doi:10.1016/j.neuron.2013.12.009

37. Karch CM, Prudencio M, Winkler DD, Hart PJ, Borchelt DR (2009) Role of mutant SOD1 disulfide oxidation and aggregation in the pathogenesis of familial ALS. Proc Natl Acad Sci U S A 106:7774-7779. doi:10.1073/pnas.0902505106

38. Kiaei M, Kipiani K, Calingasan NY, Wille E, Chen J, Heissig B, Rafii S, Lorenzl S, Beal MF (2007) Matrix metalloproteinase-9 regulates TNF-alpha and FasL expression in neuronal, glial cells and its absence extends life in a transgenic mouse model of amyotrophic lateral sclerosis. Exp Neurol 205:74-81. doi:10.1016/j.expneurol.2007.01.036

39. Lalancette-Hebert M, Sharma A, Lyashchenko AK, Shneider NA (2016) Gamma motor neurons survive and exacerbate alpha motor neuron degeneration in ALS. Proc Natl Acad Sci U S A 113:E8316-E8325. doi:10.1073/pnas.1605210113

40. Lobsiger CS, Boillee S, McAlonis-Downes M, Khan AM, Feltri ML, Yamanaka K, Cleveland DW (2009) Schwann cells expressing dismutase active mutant SOD1 unexpectedly slow disease progression in ALS mice. Proc Natl Acad Sci U S A 106:4465-4470. doi:10.1073/pnas.0813339106

41. Lobsiger CS, Boillée S, Cleveland DW (2007) Toxicity from different SOD1 mutants dysregulates the complement system and the neuronal regenerative response in ALS motor neurons. Proc Natl Acad Sci U S A 104:7319-7326. doi:10.1073/pnas.0702230104

42. Longair MH, Baker DA, Armstrong JD (2011) Simple Neurite Tracer: open source software for reconstruction, visualization and analysis of neuronal processes. Bioinformatics 27:2453-2454. doi:10.1093/bioinformatics/btr390

43. Lorenzo LE, Barbe A, Portalier P, Fritschy JM, Bras H (2006) Differential expression of GABAA and glycine receptors in ALS-resistant vs. ALS-vulnerable motoneurons: possible implications for selective vulnerability of motoneurons. Eur J Neurosci 23:3161-3170. doi:10.1111/j.1460-9568.2006.04863.x

44. Ma L, Ostrovsky H, Miles G, Lipski J, Funk GD, Nicholson LF (2006) Differential expression of group I metabotropic glutamate receptors in human motoneurons at low and high risk of degeneration in amyotrophic lateral sclerosis. Neuroscience 143:95-104. doi:10.1016/j.neuroscience.2006.07.058

45. Maher P, Schubert D (2000) Signaling by reactive oxygen species in the nervous system. Cell Mol Life Sci 57:1287-1305

46. McMurray CT (2000) Neurodegeneration: diseases of the cytoskeleton? Cell Death Differ 7:861-865. doi:10.1038/sj.cdd.4400764

47. Morisaki Y, Niikura M, Watanabe M, Onishi K, Tanabe S, Moriwaki Y, Okuda T, Ohara S, Murayama S, Takao M, Uchida S, Yamanaka K, Misawa H (2016) Selective Expression of Osteopontin in ALS-resistant Motor Neurons is a Critical Determinant of Late Phase Neurodegeneration Mediated by Matrix Metalloproteinase-9. Sci Rep 6:27354. doi:10.1038/srep27354

48. Munnamalai V, Suter DM (2009) Reactive oxygen species regulate F-actin dynamics in neuronal growth cones and neurite outgrowth. J Neurochem 108:644-661. doi:10.1111/j.1471-4159.2008.05787.x

49. Nicholson SJ, Witherden AS, Hafezparast M, Martin JE, Fisher EM (2000) Mice, the motor system, and human motor neuron pathology. Mamm Genome 11:1041-1052

50. Nimchinsky EA, Young WG, Yeung G, Shah RA, Gordon JW, Bloom FE, Morrison JH, Hof PR (2000) Differential vulnerability of oculomotor, facial, and hypoglossal nuclei in G86R superoxide dismutase transgenic mice. J Comp Neurol 416:112-125

51. Offen D, Barhum Y, Melamed E, Embacher N, Schindler C, Ransmayr G (2009) Spinal cord mRNA profile in patients with ALS: comparison with transgenic mice expressing the human SOD-1 mutant. J Mol Neurosci 38:85-93. doi:10.1007/s12031-007-9004-z

52. Pasinelli P, Brown RH (2006) Molecular biology of amyotrophic lateral sclerosis: insights from genetics. Nat Rev Neurosci 7:710-723. doi:10.1038/nrn1971

53. Perrin FE, Boisset G, Docquier M, Schaad O, Descombes P, Kato AC (2005) No widespread induction of cell death genes occurs in pure motoneurons in an amyotrophic lateral sclerosis mouse model. Hum Mol Genet 14:3309-3320. doi:10.1093/hmg/ddi357

54. Piccione EA, Sletten DM, Staff NP, Low PA (2015) Autonomic system and amyotrophic lateral sclerosis. Muscle Nerve 51:676-679. doi:10.1002/mus.24457

55. Pun S, Santos AF, Saxena S, Xu L, Caroni P (2006) Selective vulnerability and pruning of phasic motoneuron axons in motoneuron disease alleviated by CNTF. Nat Neurosci 9:408-419. doi:10.1038/nn1653

56. Raivich G, Bohatschek M, Da Costa C, Iwata O, Galiano M, Hristova M, Nateri AS, Makwana M, Riera-Sans L, Wolfer DP, Lipp HP, Aguzzi A, Wagner EF, Behrens A (2004) The AP-1 transcription factor c-Jun is required for efficient axonal regeneration. Neuron 43:57-67. doi:10.1016/j.neuron.2004.06.005

57. Saccon RA, Bunton-Stasyshyn RK, Fisher EM, Fratta P (2013) Is SOD1 loss of function involved in amyotrophic lateral sclerosis? Brain 136:2342-2358. doi:10.1093/brain/awt097

58. Saris CG, Groen EJ, van Vught PW, van Es MA, Blauw HM, Veldink JH, van den Berg LH (2013) Gene expression profile of SOD1-G93A mouse spinal cord, blood and muscle. Amyotrophic lateral sclerosis & frontotemporal degeneration 14:190-198. doi:10.3109/21678421.2012.749914

59. Saxena S, Cabuy E, Caroni P (2009) A role for motoneuron subtype-selective ER stress in disease manifestations of FALS mice. Nat Neurosci 12:627-636. doi:10.1038/nn.2297

60. Schaefer AM, Sanes JR, Lichtman JW (2005) A compensatory subpopulation of motor neurons in a mouse model of amyotrophic lateral sclerosis. J Comp Neurol 490:209-219. doi:10.1002/cne.20620

61. Strang KH, Goodwin MS, Riffe C, Moore BD, Chakrabarty P, Levites Y, Golde TE, Giasson BI (2017) Generation and characterization of new monoclonal antibodies targeting the PHF1 and AT8 epitopes on human tau. Acta Neuropathol Commun 5:58. doi:10.1186/s40478-017-0458-0

62. Synofzik M, Fernández-Santiago R, Maetzler W, Schöls L, Andersen PM (2010) The human G93A SOD1 phenotype closely resembles sporadic amyotrophic lateral sclerosis. J Neurol Neurosurg Psychiatry 81:764-767. doi:10.1136/jnnp.2009.181719

63. Takamiya R, Takahashi M, Park YS, Tawara Y, Fujiwara N, Miyamoto Y, Gu J, Suzuki K, Taniguchi N (2005) Overexpression of mutated Cu,Zn-SOD in neuroblastoma cells results in cytoskeletal change. Am J Physiol Cell Physiol 288:C253-259. doi:10.1152/ajpcell.00014.2004

64. Thannickal VJ, Fanburg BL (2000) Reactive oxygen species in cell signaling. Am J Physiol Lung Cell Mol Physiol 279:L1005-1028

65. Tjust AE, Brannstrom T, Pedrosa Domellof F (2012) Unaffected motor endplate occupancy in eye muscles of ALS G93A mouse model. Front Biosci (Schol Ed) 4:1547-1555

66. Tsujino H, Kondo E, Fukuoka T, Dai Y, Tokunaga A, Miki K, Yonenobu K, Ochi T, Noguchi K (2000) Activating transcription factor 3 (ATF3) induction by axotomy in sensory and motoneurons: A novel neuronal marker of nerve injury. Mol Cell Neurosci 15:170-182. doi:10.1006/mcne.1999.0814

67. Vlug AS, Teuling E, Haasdijk ED, French P, Hoogenraad CC, Jaarsma D (2005) ATF3 expression precedes death of spinal motoneurons in amyotrophic lateral sclerosis-SOD1 transgenic mice and correlates with c-Jun phosphorylation, CHOP expression, somato-dendritic ubiquitination and Golgi fragmentation. Eur J Neurosci 22:1881-1894. doi:10.1111/j.1460-9568.2005.04389.x

68. Wang J, Farr GW, Zeiss CJ, Rodriguez-Gil DJ, Wilson JH, Furtak K, Rutkowski DT, Kaufman RJ, Ruse CI, Yates JR, Perrin S, Feany MB, Horwich AL (2009) Progressive aggregation despite chaperone associations of a mutant SOD1-YFP in transgenic mice that develop ALS. Proc Natl Acad Sci U S A 106:1392-1397. doi:10.1073/pnas.0813045106

69. Wang J, Slunt H, Gonzales V, Fromholt D, Coonfield M, Copeland NG, Jenkins NA, Borchelt DR (2003) Copper-binding-site-null SOD1 causes ALS in transgenic mice: aggregates of non-native SOD1 delineate a common feature. Hum Mol Genet 12:2753-2764. doi:10.1093/hmg/ddg312

70. Wang L, Sharma K, Grisotti G, Roos RP (2009) The effect of mutant SOD1 dismutase activity on non-cell autonomous degeneration in familial amyotrophic lateral sclerosis. Neurobiol Dis 35:234-240. doi:10.1016/j.nbd.2009.05.002

71. Williamson TL, Cleveland DW (1999) Slowing of axonal transport is a very early event in the toxicity of ALS-linked SOD1 mutants to motor neurons. Nat Neurosci 2:50-56. doi:10.1038/4553

72. Yamanaka K, Boillee S, Roberts EA, Garcia ML, McAlonis-Downes M, Mikse OR, Cleveland DW, Goldstein LS (2008) Mutant SOD1 in cell types other than motor neurons and

oligodendrocytes accelerates onset of disease in ALS mice. Proc Natl Acad Sci U S A 105:7594-7599. doi:10.1073/pnas.0802556105

73. Yu L, Guan Y, Wu X, Chen Y, Liu Z, Du H, Wang X (2013) Wnt Signaling is altered by spinal cord neuronal dysfunction in amyotrophic lateral sclerosis transgenic mice. Neurochem Res 38:1904-1913. doi:10.1007/s11064-013-1096-y

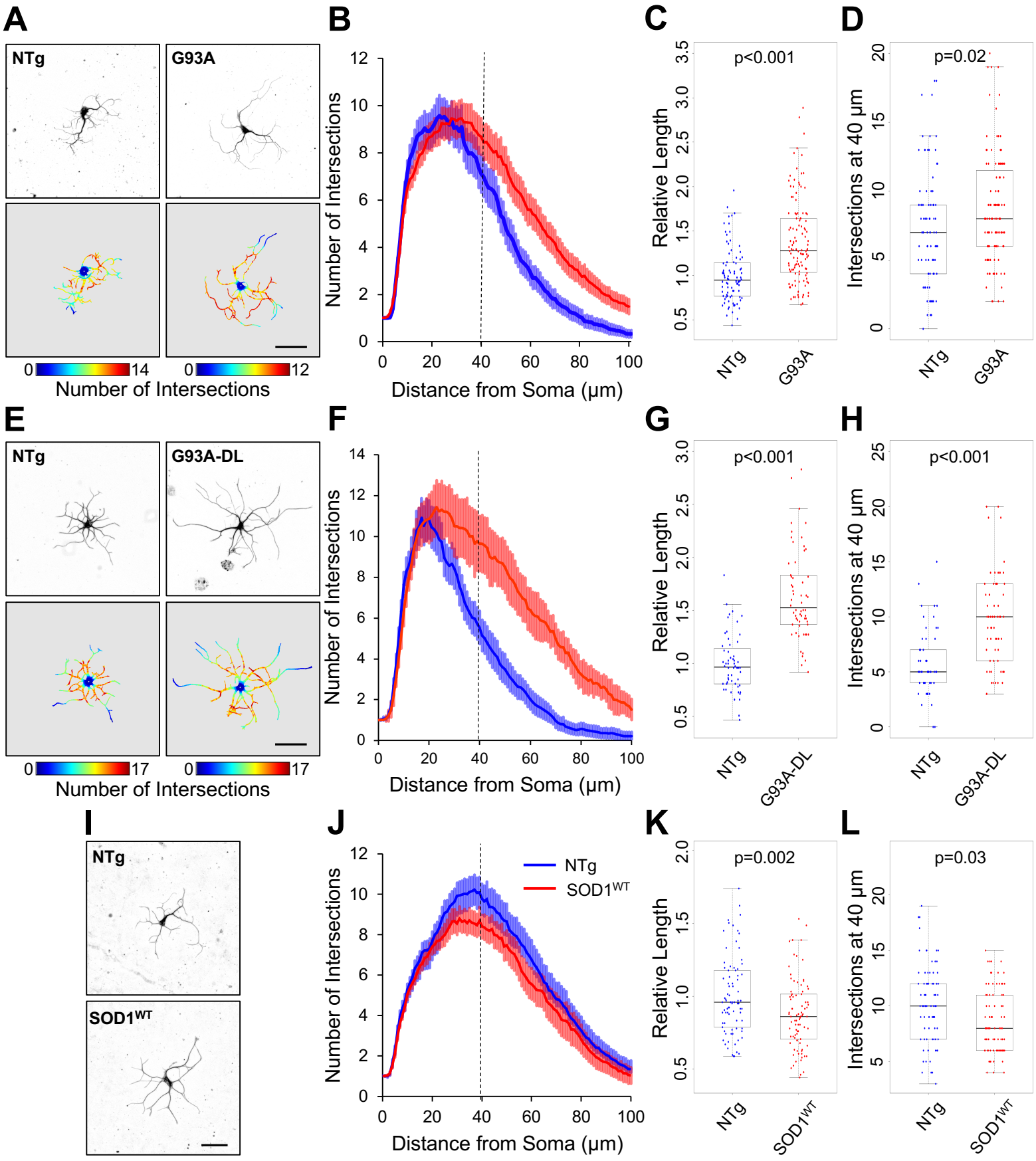

Figure 1

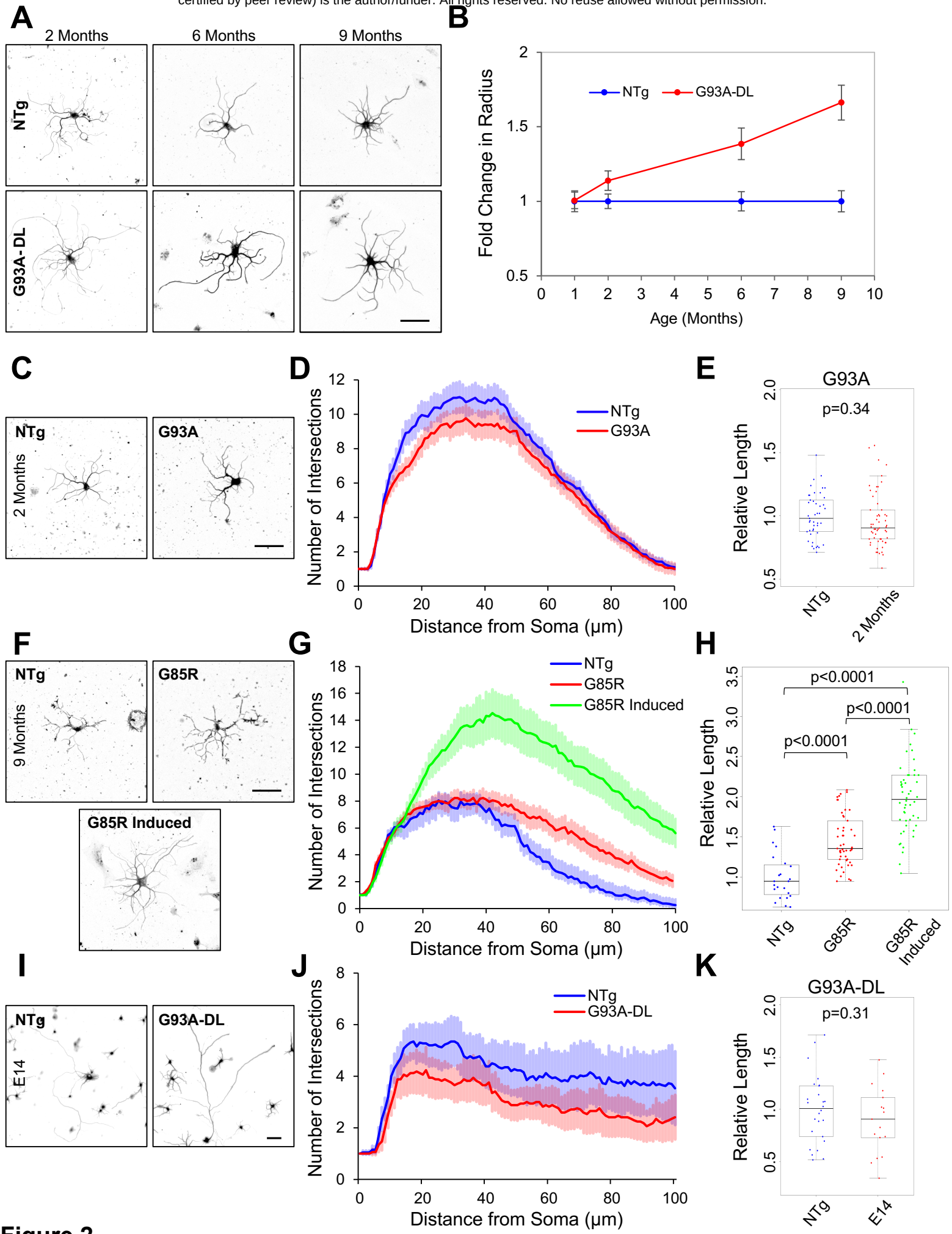

Figure 2

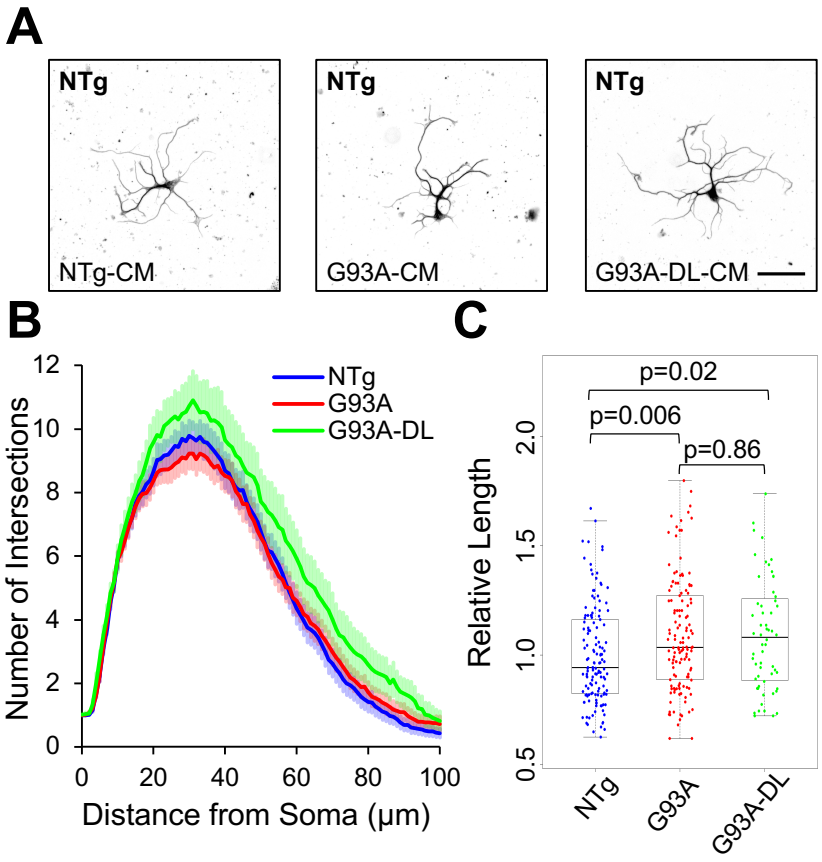

Figure 3

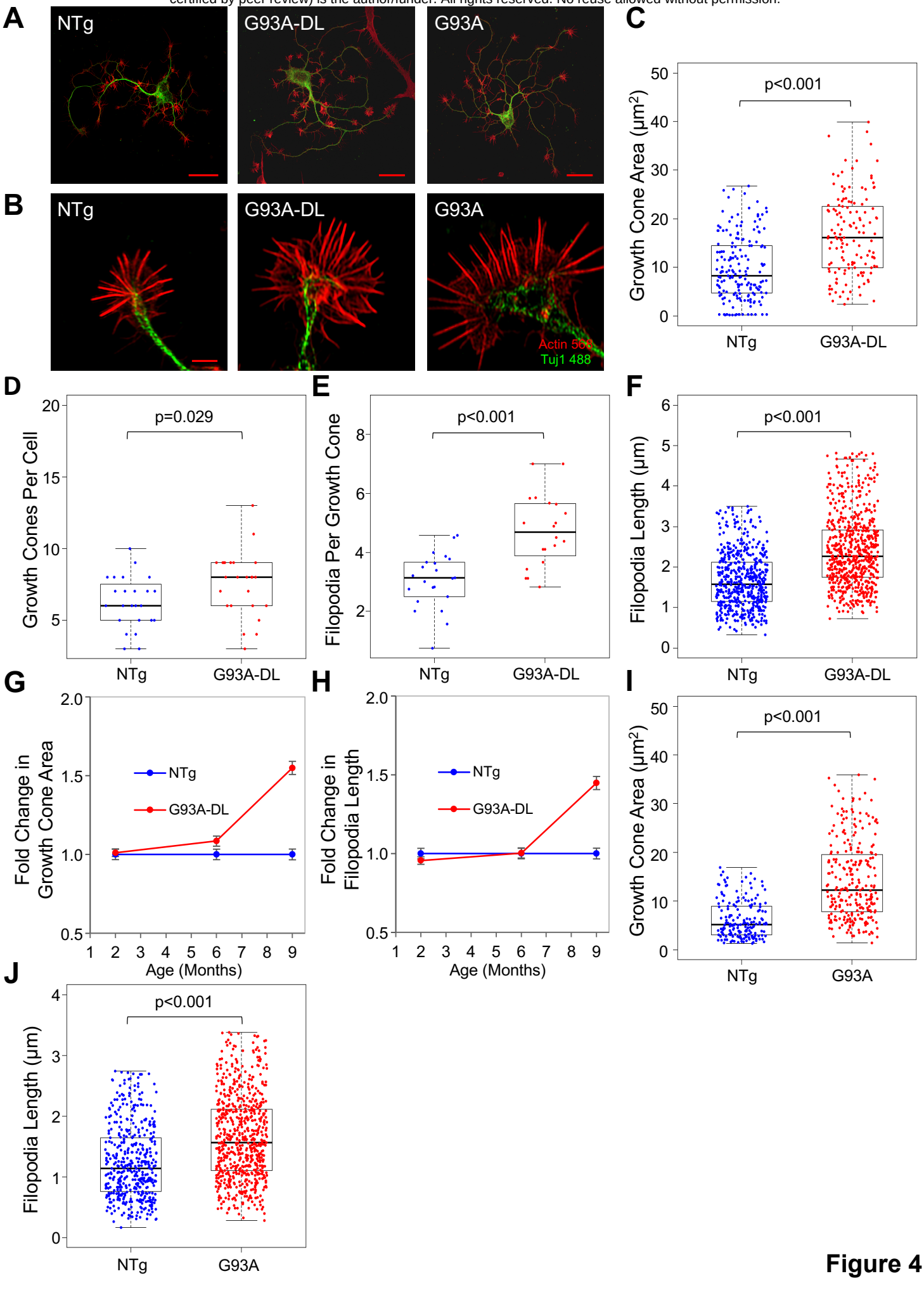

Figure 4